ARTICLES

The Nonlinear Optical Properties of the Crystal (*S*)-3-Methyl-5-nitro-*N*-(1-phenylethyl)-2-pyridinamine

S. Lochran, R. T. Bailey, F. R. Cruickshank,* D. Pugh, J. N. Sherwood, and G. S. Simpson
Department of Pure and Applied Chemistry, University of Strathclyde, 295 Cathedral Street, Glasgow G1 1XL, U.K.

P. J. Langley
Centre for Materials Research, School of Physical Sciences, The University of Kent, Canterbury, Kent CT2 7NH, U.K.

J. D. Wallis
Department of Chemistry and Physics, Nottingham Trent University, Clifton Lane, Nottingham NG11 8NS, U.K.

Received: November 17, 1999; In Final Form: April 10, 2000

The organic crystal (*S*)-3-methyl-5-nitro-*N*-(1-phenylethyl)-2-pyridinamine has been previously identified by the powder technique as a promising nonlinear optical material. Large single crystals ($3 \times 3 \times 2$ cm^3) of this material have been grown by temperature lowering of a seeded supersaturated solution in acetone. Refined refractive indices were obtained from the predicted angles of incidence of the phase-matched second harmonic signals. Second-order nonlinear optical coefficients, d_{ij}, as measured by the Maker fringe technique, are 11, 9, and 7 pm V^{-1} for d_{14}, d_{25}, and d_{36}, respectively. The results are compared with calculations based on the oriented gas model.

Introduction

In recent years there has been considerable interest in the use of molecular crystals of conjugated organic compounds for frequency converters and optical modulators because they generally exhibit nonlinear optical properties that surpass those of current inorganic materials. They have a wide range of applications that include optical data storage, communications, and optical computing systems. (*S*)-5-Nitro-*N*-(1-phenylethyl)-2-pyridinamine (MBANP) is a molecular organic crystal, the nonlinear optical properties of which have been extensively studied,[1−5] and the organic material (*S*)-3-methyl-5-nitro-*N*-(1-phenylethyl)-2-pyridinamine (S3MeMBANP)[1,6] is a derivative of this compound with a methyl group substituted in the 3 position of the nitropyridine ring (see Figure 1a). The molecular structure of MBANP is given in Figure 1b for comparison. S3MeMBANP was tested for second harmonic generation by the powder technique[7,8] and showed a signal 16 times that of urea, which compares with the previously reported[1] value of 7 times that of urea and illustrates the uncertainties associated with the powder technique.[9,10] Derivatives of MBANP have received little attention, although the powder tests conducted by Tweig et al.[1] showed that some of these derivatives were efficient at second harmonic generation (SHG).

So that a full optical assessment of its performance can be made, large single crystals of this material have been grown by the temperature-lowering technique and the subsequent preparation of optical quality orientated specimens has been carried out. In this paper we extend the previous study[6] of the linear optics, present the results of the first study of the nonlinear optical properties of an MBANP derivative, and compare the results with those of calculations using the oriented gas model.

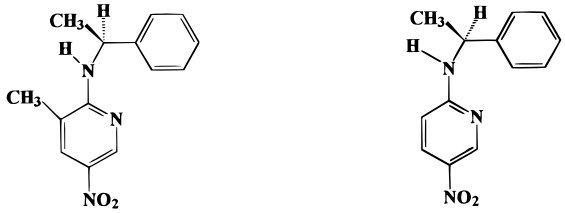

Figure 1. Molecular structures of (a) S3MeMBANP and (b) MBANP. Note: The structures of the two molecules differ only by the methyl group on the pyridine ring.

Crystal Growth and Sample Preparation

Growth of high-quality single crystals is largely dependent on the purity of the starting material. S3MeMBANP was purified to 99.98% by continuous-column chromatography.[6] Single crystals of this material can be grown by the Bridgman technique and from a solution of acetone by the temperature-lowering technique. Crystals were grown to a maximum size of $3 \times 3 \times 2$ cm^3 by this latter method and a more detailed description of the crystal growth procedure has been reported elsewhere.[6] The crystals grown by this method were examined for defect concentration by X-ray topography.[6] This showed that, despite the accelerated growth, there existed large areas essentially free

10.1021/jp994086y CCC: $19.00 © 2000 American Chemical Society
Published on Web 07/01/2000

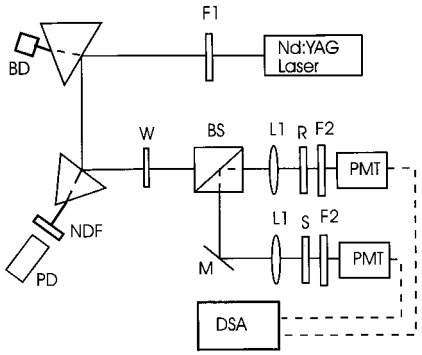

Figure 2. Experimental apparatus for the collection and recording of Maker fringes and the analysis of phase matching properties. W, 1064 nm narrow band-pass filter; F2, 532 narrow band-pass filter; F1, half-wave plate; BS, 50−50 beam splitter; L1, 50 cm focal length lens; M, dielectric mirror; NDF, neutral density filter; PD, high-speed photodiode; R, quartz reference; S, sample; PMT, photomultiplier tube; DSA, digitizing signal analyzer; BD, beam dump.

of defects. Samples for this work were prepared from crystals oriented by means of a Laue camera and were cut from a defect-free zone of the parent crystal with a solvent saw. The specimens were then polished by using a Logitech PM-2 polishing machine, which is capable of polishing these materials to a flatness of $\lambda/5$ of Na light and to a parallelism of 30 s of arc.

S3MeMBANP belongs to the orthorhombic system $P2_12_12_1$ with point group 222 and unit cell parameters $a = 5.481(4)$ Å, $b = 6.791(8)$ Å, and $c = 35.88(3)$ Å at room temperature with four molecules per unit cell and a calculated density of 1.28 g cm^{-3}.

Maker Fringes

Of the second-order tensor, $\chi^{(2)}$, in the relationship between second-order polarizability, $P^{2\omega}$, and the electrical field of the laser, E^{ω}, at the fundamental frequency, ω,

$$\begin{bmatrix} P_x^{2\omega} \\ P_y^{2\omega} \\ P_z^{2\omega} \end{bmatrix} = \epsilon_0 \begin{bmatrix} d_{11} & d_{12} & d_{13} & d_{14} & d_{15} & d_{16} \\ d_{21} & d_{22} & d_{23} & d_{24} & d_{25} & d_{26} \\ d_{31} & d_{32} & d_{33} & d_{34} & d_{35} & d_{36} \end{bmatrix} \begin{bmatrix} (E_x^{\omega})^2 \\ (E_y^{\omega})^2 \\ (E_z^{\omega})^2 \\ 2(E_y^{\omega}E_z^{\omega}) \\ 2(E_z^{\omega}E_x^{\omega}) \\ 2(E_x^{\omega}E_y^{\omega}) \end{bmatrix} \quad (1)$$

the d_{ij} are the second-order nonlinear optical coefficients and only the elements d_{14}, d_{25}, and d_{36}, are nonzero. The subscripts x, y, and z refer to the piezoelectric axis set. The relationship between the induced second-order polarization $P^{(2)}$ and the applied electric field E for this material is therefore given by

$$\begin{aligned} P_x^{(2)} &= 2\epsilon_0 d_{14} E_y E_z \\ P_y^{(2)} &= 2\epsilon_0 d_{25} E_x E_z \\ P_z^{(2)} &= 2\epsilon_0 d_{36} E_x E_y \end{aligned} \quad (2)$$

where ϵ_0 is the permittivity of free space. Measurement of these nonlinear optical coefficients was made by the Maker fringe technique.[11] The apparatus is shown in Figure 2. This experiment consists of rotating an optically flat, plane, parallel slab of the nonlinear material in question so that the polarization of the laser and the analysis of the appropriate nonlinear polarization yield the desired coefficient in accordance with eq 2. For example, to measure d_{14}, a specimen was oriented, cut, and polished such that the Y and Z dielectric axes made an accurately known angle of approximately 45° to the input face of the crystal blank. The pulsed Nd:YAG laser was polarized in the $Y-Z$ plane and the analysis of the intensity of the second harmonic output with polarization parallel to the X dielectric axis yielded d_{14}.

As the crystal rotates, the path lengths traversed in it by the bound (nonlinear polarization) and free (induced electromagnetic wave at 2ω) waves change so that there is constructive and destructive interference between them. The resulting variation of the generated second harmonic intensity as a function of angle of incidence exhibits a fringe pattern as the relative phases of the bound and free waves change. The signal obtained for each angle of incidence at typically 0.2° intervals is averaged over 64 experiments and ratioed against the signal from an orientated quartz crystal set to the first Maker fringe of its d_{11} value, thus normalizing to the laser power. The appropriate d_{ij} value is calculated from the intensity of the second harmonic radiation at normal incidence. The observed intensity at this incidence angle could take any value from zero to the required value because it depends on the thickness of the specimen and the interference pattern resulting from it. Therefore, the true intensity has to be calculated at the center of the appropriate envelope function of the fringe pattern from values observed at nonzero incidence angles.

For the case in which the input polarization is extraordinary (dependent on the angle of incidence) and the second harmonic polarization is ordinary (independent of the incidence angle), the function resulting from the interference of the free and bound waves has the form of $\sin^2 \varphi$ with φ given by

$$\varphi \frac{2\pi L}{\lambda}(n_o^{2\omega} - n_e^{\omega}(\theta_\omega)) \quad (3)$$

L is the sample thickness and λ is the wavelength of the fundamental beam. In the case of the measurement of d_{25}, the ordinary polarization is parallel to the rotation axis Y and the extraordinary polarization is in the XZ dielectric plane The envelope of the angular dependence of the second harmonic, $I_{2\omega}$, is then described by the function[12]

$$I_{2\omega} = \frac{8\pi c (E_\omega)^4 d^2}{[(n_y^{2\omega})^2 - (n_{xy}^{\omega}(\theta_\omega))^2]^2}\left[\frac{n_z^2}{n_x^2}\sin(2\theta'_\omega)\right]^2 t_\omega^4(\theta_\omega) T_{2\omega}(\theta_\omega) \quad (4)$$

where

$$t_\omega = \frac{2n_{xz}^{\omega}(\theta_\omega)\cos(\theta_\omega)}{(n_z^{\omega})^2 \cos\theta_\omega + n_{xz}^{\omega}(\theta_\omega)\cos(\theta'_\omega)} \quad (5)$$

and

$$T_{2\omega} = 2n_y^{2\omega}\cos(\theta'_{2\omega}) \frac{(\cos\theta_\omega + n_{xz}^{\omega}\cos(\theta'_\omega))(n_y^{2\omega}\cos(\theta'_{2\omega}) + n_{xz}^{\omega}\cos(\theta'_\omega))}{(n_y^{2\omega}\cos(\theta'_{2\omega}) + \cos\theta_\omega)^3} \quad (6)$$

$(\theta'_{2\omega})$ is the second harmonic free-wave propagation vector angle with the X direction. The value of the refractive index of the extraordinary ray is dependent on the angle of incidence and is calculated from

$$\frac{1}{n_{xz}^2} = \frac{\cos^2 \theta'_\omega}{n_z^2} + \frac{\sin^2 \theta'_\omega}{n_x^2} \tag{7}$$

In practice, the second harmonic envelope function of the signal is ratioed against the normal incidence signal from the corresponding envelope for a quartz crystal placed at the sample position. This leaves only the refractive index functions to be determined to yield the square of the ratio of the d coefficient of the sample to the d_{11} coefficient of quartz.

Nonzero minima of Maker fringes, indicating incompletely destructive interference, can be due to a number of factors. First, the surface of the specimen must be polished flat to a fraction of a coherence length to obtain perfect zeroes. The coherence lengths of organic crystals are often very short (typically 0.3−2.0 μm) in comparison with that of quartz (20 μm), so that this quality of finish becomes unattainable. Second, the softer nature of organic crystals and the well defined cleavage planes also make the required finish much harder to obtain.

Maker fringes in S3MeMBANP have proved difficult to obtain because this material possesses very powerful phase matching in various orientations that masks the fringes in all but one orientation. Therefore, it is possible to measure only the d_{25} coefficient directly. However, this coefficient was measured by using two different orientations. In the first orientation an optical blank was prepared with the X and Z dielectric axes at approximately 45° to the input (107) face and the Y dielectric axis as the rotation axis. This configuration resulted in the production of symmetrical Maker fringes that maximized at the center.

In the second orientation, the d_{25} coefficient was measured by making use of the natural cleavage plane, (001), and rotating about the Y dielectric axis. This yielded an off-axis set of Maker fringes that is shown in Figure 3. The reasons for nonzero minima discussed above do not account entirely for the nonzero minima in this sample. It is believed that the nonzero minima arise principally because this material possesses such strong phase matching that a background of second harmonic radiation contributes to the observed fringe signal. Therefore, the zero correction suggested by Kurtz and Perry, and that we normally use, is essentially invalid in this case and thus not used.

In an attempt to establish the reproducibility of the d_{ij} coefficients in organic nonlinear optical crystals, the measurement of d_{25} in this work was repeated several times with each sample at different sites on the input face. The values obtained varied by ±2.4 pm V^{-1} (±27% for d_{25}). A typical plot of the Maker fringes from the (107) sample is shown in Figure 4.

From the Maker fringes on each sample, the d_{25} value obtained was 15 pm V^{-1} averaged over the sets of fringes obtained from both orientations. It should be noted that instead of the value of d_{11} = 0.5 pm V^{-1} for quartz[13] used in the calculation of previous data,[14] the presently accepted[15,16] value of 0.3 pm V^{-1} is used in this work.

Refractive indices at 1.064 μm were refined by correlating observed with calculated phase matching angles and are given in Table 1 together with slightly improved Sellmeier curve fits incorporating earlier data.[6] The coherence length of a material at normal incidence is given by

$$l_c = \frac{\lambda}{4|n_\omega - n_{2\omega}|} \tag{8}$$

The coherence lengths of S3MeMBANP in the various directions in which Maker fringes were obtained are given in Table 1. As can be seen from the table, the coherence lengths for this material are very short. This confirms that the finish required to obtain good zeroes in a Maker fringe would be beyond the capability of most polishing technology. Coupled

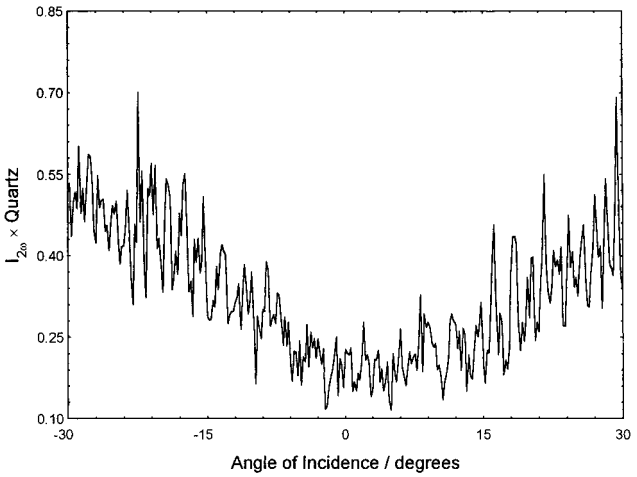

Figure 3. Maker fringes obtained from a cleaved (001) sample. The nonzero minima are due to a combination of imperfect surfaces and background phase matching.

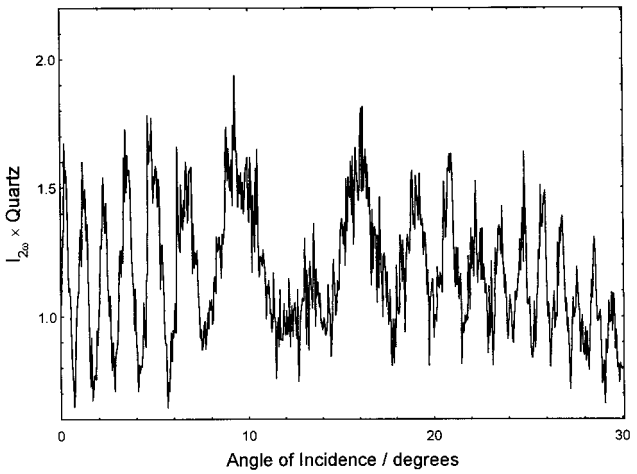

Figure 4. Maker fringes obtained from a (107) sample.

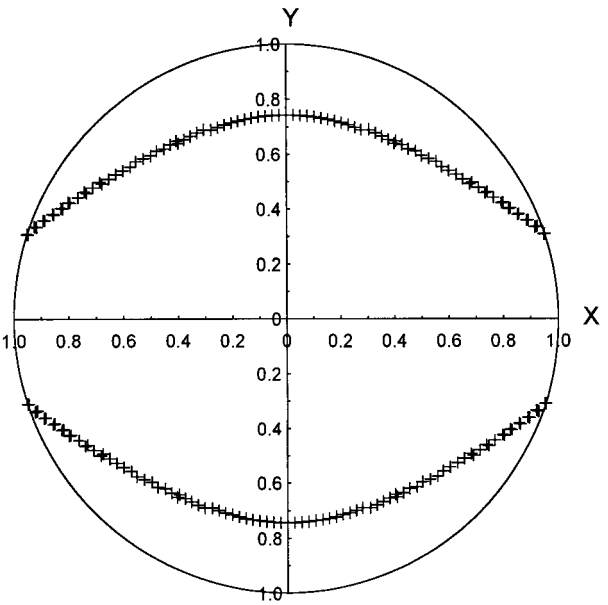

Figure 5. Stereographic projection onto the XY plane of the phase-matching locus.

TABLE 1

	ω	2ω	Sellmeier coefficients (λ in μm)[a]
n_x	1.5893	1.6899	$A = 2.67839$, $B = 0.0919939$, $C = 0.175789$, $D = 0.230901$
n_y	1.7365	1.8999	$A = 2.35431$, $B = 0.581332$, $C = 0.152215$, $D = 0.00922734$
n_z	1.6502	1.7253	$A = 2.63522$, $B = 0.153796$, $C = 0.163522$, $D = 0.0811653$
	l_c (001)[b]		0.85 μm
	l_c (107)[b]		0.95 μm

[a] The form of the Sellmeier equation used is $n_i^2 = A + B\lambda^2/\lambda^2 - C) - D\lambda^2$. [b] Coherence lengths are quoted for a fundamental wavelength of 1.064 μm.

TABLE 2

orientation	experimental position/deg	theoretical position/deg
(101)[a]	31.5	32.2
(110)	49	42.4
special 38° blank[b]	19.4	17.1

[a] For rotation of this blank about the $Z-X$ axis. [b] See text.

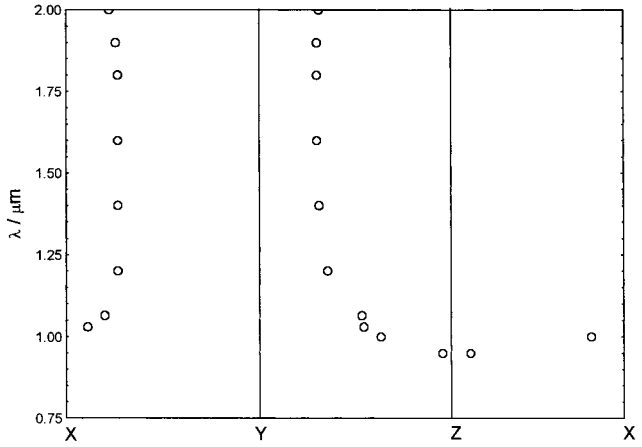

Figure 6. Phase matching curves as a function of wavelength.

with the fact that strong phase matching is present, this accounts for the nonzero minima in fringes produced by this compound.

Phase-Matching Properties

The observed angles of incidence of the phase-matched signals can be correlated with the predicted positions. Since the predictions make use of the refractive indices at ω and 2ω, further refinements of the refractive indices are possible by altering their values slightly until the predicted positions coincide with those observed. Experimental and predicted phase-matched positions are given in Table 2. As can be seen from Table 2, the positions of the experimental and theoretical signals coincide within a few degrees. A change in the refractive index of 0.001 can produce a change in the predicted positions of several degrees. A stereographic projection of the phase-matching locus at 1.064 μm is shown in Figure 5, which was constructed by using the refractive indices refined in this work. It should be noted that only Type I phase matching is possible in this compound.

Phase-matching loci in the principal planes as a function of wavelength are shown in Figure 6. Two striking features of this figure show that this material is potentially ideal for several applications. First, the rather vertical nature of part of the curve shows that this material can be phase matched at the same angle over a wide range of wavelengths. This wavelength noncritical phase matching occurs at 20° from the X dielectric axis in the $X-Y$ plane and at 20° from the Y axis in the $Y-Z$ plane for wavelengths from around 1200−2000 nm and possibly beyond. This would allow the frequency doubling of a tunable infrared laser source, such as an optical parametric oscillator or an IR dye laser, without retuning the phase matching angle of the doubling crystal.Second, there exists a portion of this curve in which, for a specific narrow band wavelength range around 950 nm, phase matching is possible over a wide range of angles. This angle noncritical phase matching has two very important consequences. First, when a material is angle-noncritically phase matched, walk-off does not exist between the bound polarization wave and the free second harmonic wave. This has the effect of increasing conversion efficiency, particularly for tightly focused beams. Second, one propagation direction needed for this condition is the Z dielectric axis, which is orthogonal to a natural cleavage plane (001) of S3MeMBANP. This has the advantage that very high quality optical specimens can be readily obtained with little need for optical polishing.

A measurement of the remaining d_{ij} coefficients can be made from the amplitude of phase-matched signals when the Maker fringes are too distorted by phase-matched signals to be useful. The amplitude of the phase-matched signal relative to quartz is given by

$$\frac{I_s^{2\omega}}{I_r^{2\omega}} = \frac{4\pi^2 L^2}{\lambda^2}\left(\frac{d_s}{d_{Qtz}}\right)^2 \frac{t_\omega^{\,4} T_{2\omega}}{(2n_\omega \cos\theta'_{PM})^2} \times \left[\frac{(1+n_{Qtz}^{\,\omega})^3(1+n_{Qtz}^{\,2\omega})^3(n_{Qtz}^{\,\omega}-n_{Qtz}^{\,2\omega})^2(n_{Qtz}^{\,\omega}+n_{Qtz}^{\,2\omega})}{n_{Qtz}^{\,2\omega}}\right] \quad (9)$$

and is derived in the Appendix. With this equation, d_{14} was measured from the amplitude of the phase-matched signal. An optical blank was finished to the tolerances described above for Maker fringes and so oriented that the normal to the blank made an angle of 38° with the Z axis and the incidence plane was parallel with the $Y-Z$ plane. The signal was observed when this optical blank was rotated about the X axis. The value of d_{14} obtained was 11 pm V $^{-1}$. In the case of d_{14} the phase-matched signal was found to occur at an angle of incidence of 19.4° with a peak intensity of 1.18×10^8 times that of the quartz Maker fringe and is shown in Figure 7.

Measurement of the value of d_{36} was carried out from the peak of a phase-matched signal from a (110) plane rotated about the Z dielectric axis by using the same analysis as before. A schematic diagram of the configuration used is given in Figure 8.

Phase matching was observed in this sample at an angle of incidence of 48.2° with an intensity equal to 7.55×10^6 times that of the quartz Maker fringe. A plot of the signal is shown in Figure 9.

With the peak of the phase-matched signal occurring at an external angle of incidence of 48.2°, the value of the effective d coefficient obtained was $d_{eff} = 2.9$ pm V^{-1}. Since measurements of nonlinear coefficients are made relative to the

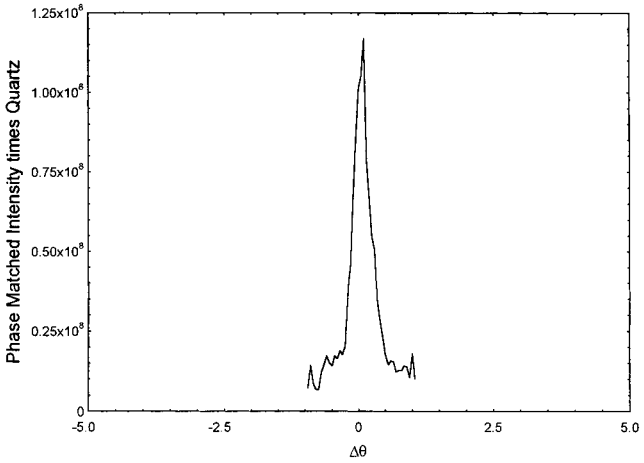

Figure 7. Phase-matched signal with a peak intensity of 1.18×10^8 times quartz. The signal is 0.3° wide at fwhm.

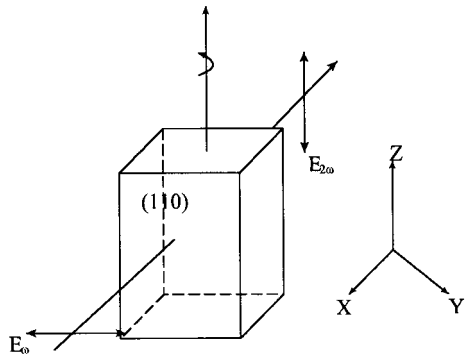

Figure 8. Schematic diagram of experimental configuration for the determination of d_{36} from phase matching in S3MeMBANP.

piezoelectric axis set, the internal angles must be calculated with reference to this axis set. The value of d_{36} was found to be 7 pm V^{-1}.

The point group of S3MeMBANP is 222 and therefore the nonlinear $\chi^{(2)}$ tensor has the contracted form

$$d_{ij} = \begin{bmatrix} 0 & 0 & 0 & 11 & 0 & 0 \\ 0 & 0 & 0 & 0 & 9 & 0 \\ 0 & 0 & 0 & 0 & 0 & 7 \end{bmatrix} \quad (10)$$

Hyperpolarizability Calculations

The approach commonly adopted to produce a theoretical $\chi^{(2)}$ tensor for molecular crystals is to calculate a molecular hyperpolarizability tensor, β, by quantum theory and combine the molecular contributions to yield a crystal susceptibility tensor using the oriented gas model.[17] Although the concepts used are relatively simple, there is evidence that they can give reliable results in the few cases where there are sufficient data to test them. While the quantum calculations give reasonable values of the nonlinearities for one molecule relative to another, they cannot be expected to give the molecular hyperpolarizability tensors with the same confidence. The oriented gas model corrects for internal fields by considering the molecules to be in cavities in dilute media and ignores the strong permanent electric fields present in a real, dense crystal. The nonlinear optical coefficients can then be expressed by

$$d_{IJK} = \frac{N}{n(g)} f_I^{2\omega} f_J^{\omega} f_K^{\omega} \sum_s^{n(g)} \cos(\theta_I^s) \cos(\theta_J^s) \cos(\theta_K^s) \beta \quad (11)$$

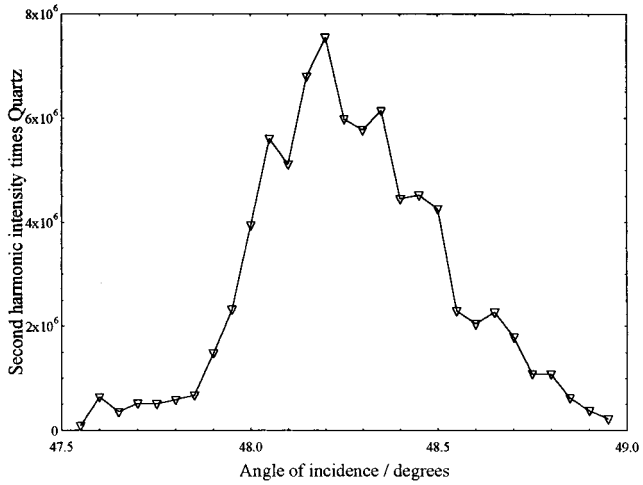

Figure 9. Phase-matched signal in S3MeMBANP obtained from the (110) plane. The peak intensity is 7.55×10^6 times quartz and the width is 0.5° at fwhm. Thickness = 5.317 mm.

where s is the number of sites in the unit cell, θ_I^s are the angles between the molecular charge-transfer axis and dielectric axis, I, for molecule at site s; f_I^{ω} is the Lorentz−Lorenz local field correction given by $[(n_I^{\omega})^2 + 2]/3$; n_I^{ω} is the refractive index at wavelength ω on dielectric axis I; N is the number of molecules per unit volume; and $n(g)$ is the number of symmetry equivalent positions in the unit cell (e.g., 4 for S3MeMBANP).

Two quantum mechanical approaches have been used to calculate the molecular hyperpolarizability tensor. The first, the two-state theory, assumes that the hyperpolarizability stems from one virtual electronic transition polarized along a single charge-transfer axis. This axis is assumed to lie along the line joining the $-NH_2$ nitrogen atom to that of the $-NO_2$ group. The hyperpolarizability vector along this charge-transfer axis is resolved along the orthogonal crystal axes and summed over all molecules in the unit cell to obtain the molecular hyperpolarizability tensor. In the second approach,[18] CNDOVSB, the complete β tensor is calculated by summing over a large number of virtual excited states by using a semiempirical method. The theory is paramaterized to reproduce excited-state energies and dipoles consistent with UV/visible spectroscopy.

The two theoretical approaches result in the following $\chi^{(2)}$ tensors:

$$\text{two-state model} \qquad d_{ij} = \begin{bmatrix} 0 & 0 & 0 & 8.7 & 0 & 0 \\ 0 & 0 & 0 & 0 & 9.1 & 0 \\ 0 & 0 & 0 & 0 & 0 & 8.6 \end{bmatrix}$$

$$\text{CNDOVSB} \qquad d_{ij} = \begin{bmatrix} 0 & 0 & 0 & 15 & 0 & 0 \\ 0 & 0 & 0 & 0 & 19 & 0 \\ 0 & 0 & 0 & 0 & 0 & 15 \end{bmatrix}$$

In the two-state model, the β value (also obtained by the CNDOVSB method[18]) for the molecule along the charge-transfer axis is very similar for MBANP (14 esu) and S3MeMBANP (15.4 esu) as would be expected for methyl substitution.

Conclusions

For S3MeMBANP, the d_{25} value was measured from Maker fringe envelopes with two different crystal orientations and is 9 pm V^{-1}. The d_{14} value could not be measured from such fringes since they were obscured by residual phase-matching signals; however, from the amplitude of the phase-matched signal observed where the $Y-Z$ dielectric plane intersects the

phase-matching locus, the value of 11 pm V^{-1} was obtained. The value of d_{36} measured from phase-matching signals was 7 pm V^{-1}. These values compare with the largest value obtained for MBANP, $d_{22} = 36$ pm V^{-1}, and that of ±MBANP,[19] $d_{31} = 6.8$ pm V^{-1}. All these values are related to d_{11} quartz $= 0.3$ pm V^{-1}. For comparison purposes, earlier values have been rescaled from the quartz value of 0.5 pm V^{-1}. Given the uncertainty in measuring d_{ij} values as exemplified by the 27−36 pm V^{-1} range[3,20] for d_{22} of MBANP, it is difficult to be certain that the Kleinman conjecture is followed to better than ±25%. Although simpler, the two-state model gives better agreement with the experimental results. This is also the case with MBANP, and ±MBANP, for which the tensors obtained are respectively

two-state model (MBANP)

$$d_{ij} = \begin{bmatrix} 0 & 0 & 0 & 0.4 & 0 & 0.002 \\ 0.0006 & 55 & 23 & 0 & 0.12 & 0 \\ 0 & 0 & 0 & 21 & 0 & 0.11 \end{bmatrix}$$

CNDOVSB (MBANP)

$$d_{ij} = \begin{bmatrix} 0 & 0 & 0 & 2.7 & 0 & -7.9 \\ -13 & 62 & 28 & 0 & 3.5 & 0 \\ 0 & 0 & 0 & 27 & 0 & 2.9 \end{bmatrix}$$

and

two-state model (±MBANP)

$$d_{ij} = \begin{bmatrix} 0 & 0 & 0 & 0 & 7.3 & 0 \\ 0 & 0 & 0 & 6.4 & 0 & 0 \\ 7.1 & 6.2 & 0.54 & 0 & 0 & 0 \end{bmatrix}$$

CNDOVSB (±MBANP)

$$d_{ij} = \begin{bmatrix} 0 & 0 & 0 & 0 & 12 & 0 \\ 0 & 0 & 0 & 3.7 & 0 & 0 \\ 11 & 4.3 & -2.8 & 0 & 0 & 0 \end{bmatrix}$$

Comparing with the experimental results:

MBANP $\quad d_{ij} = \begin{bmatrix} 0 & 0 & 0 & ? & 0 & ? \\ ? & 36 & ? & 0 & ? & 0 \\ 0 & 0 & 0 & ? & 0 & ? \end{bmatrix}$

±MBANP $\quad d_{ij} = \begin{bmatrix} 0 & 0 & 0 & 0 & ? & 0 \\ 0 & 0 & 0 & ? & 0 & 0 \\ 6.8 & 4.7 & 0.84 & 0 & 0 & 0 \end{bmatrix}$

S3MeMBANP has been shown to be wavelength-noncritically phase-matchable from 1200 to 2000 nm and angle-noncritically phase matchable at 950 nm, with the readily available (001) cleavage plane within this angle range. This last result is dependent upon extrapolation of the Sellmeier relationships, which can be unreliable outside the range of wavelengths used in the measurements.

Appendix

In the paper by Jerphagnon and Kurtz,[11] the second harmonic intensity, $I_{2\omega}$, is given by

$$I_{2\omega} = \frac{512\pi^2}{c\omega^2} d^2 t_\omega^{\,4} T_{2\omega} R p^2 \frac{I_\omega^{\,2}}{(n_\omega^{\,2} - n_{2\omega}^{\,2})^2} B \sin^2 \Psi \quad \text{(A1)}$$

where

$$\Psi = \frac{2\pi L}{\lambda}(n_\omega \cos \theta_R^{\,\omega} - n_{2\omega} \cos \theta_R^{\,2\omega}) = \frac{\Delta k L}{2} \quad \text{(A2)}$$

A full description of each term is given in ref 11. Also

$$(n_\omega^{\,2} - n_{2\omega}^{\,2})^2 = \left(\frac{\Delta k L}{2}\right)^2 \left(\frac{\lambda}{2\pi L}\right)^2 (n_\omega \cos \theta_R^{\,\omega} + n_{2\omega} \cos \theta_R^{\,2\omega})^2 \quad \text{(A3)}$$

However, $(n_\omega^2 - n_{2\omega}^2)^2 = 0$ when phase matching occurs since $n_\omega = n_{2\omega}$. Therefore, the right-hand side of eq A1 will tend to infinity. Using

$$\lim_{\theta \to 0} \frac{\sin \theta}{\theta} \to 1$$

and eqs A2 and A3, eq A1 can be rewritten as

$$I_{2\omega} = \frac{512\pi^2}{c\omega^2} d^2 t_\omega^{\,4} T_{2\omega} R p^2 I_\omega^{\,2} B \times \frac{\sin^2 (\Delta k L/2)}{(\Delta k L/2)^2} \left(\frac{2\pi L}{\lambda}\right)^2 \frac{1}{(n_\omega \cos \theta_R^{\,\omega} + n_{2\omega} \cos \theta_R^{\,2\omega})^2} = \frac{2^{11}\pi^2}{c\omega^2\lambda^2} d^2 t_\omega^{\,4} T_{2\omega} R p^2 I_\omega^{\,2} B L^2 \frac{1}{(2n_\omega \cos \theta_R)^2} \quad \text{(A4)}$$

since the refractive indices and the refracted angles are equal at phase matching. For the orientation in which the nonlinear polarization is parallel to the X rotation axis and the fundamental beam is in the plane of incidence (YZ plane), the transmission factors are given by

$$t_\omega = \frac{2n_{yz}^{\,\omega} \cos \theta_\omega}{(n_y^{\,\omega})^2 \cos \theta_\omega + n_{yz}^{\,\omega} \cos \theta'_\omega} \quad \text{(A5)}$$

and

$$T_{2\omega} = 2n_x^{\,2\omega} \cos \theta'_{2\omega} \times \frac{(\cos \theta_\omega + n_{yz}^{\,\omega} \cos \theta'_\omega)(n_x^{\,2\omega} \cos \theta'_{2\omega} + n_{yz}^{\,\omega} \cos \theta'_\omega)}{(n_{yz}^{\,2\omega} \cos \theta'_{2\omega} + \cos \theta_\omega)^3} \quad \text{(A6)}$$

For quartz at normal incidence, the second harmonic intensity is given by

$$I_{Qtz}^{\,2\omega} = \frac{2^{14}\pi^2}{c\omega^2} I_\omega^{\,2} d_{Qtz}^{\,2} \times \frac{n_{2\omega}}{(1 + n_\omega)^3 (1 + n_{2\omega})^3 (n_\omega - n_{2\omega})^2 (n_\omega + n_\omega)} \quad \text{(A7)}$$

Dividing eq A4 by eq A7 gives

$$\frac{I_s^{2\omega}}{I_{Qtz}^{2\omega}} = \frac{2^{16}\pi^4\left(\frac{I_\omega^2}{c\omega^2\lambda^2}\right)d_s^2 t_\omega^4 T_{2\omega}\left(\frac{L^2}{(2n_\omega\cos\theta'_{PM})^2}\right)}{2^{14}\pi^4\left(\frac{I_\omega^2}{c\omega^2}\right)d_{Qtz}^2\left(\frac{n_{2\omega}}{(1+n_\omega)^3(1+n_{2\omega})^3(n_\omega-n_{2\omega})^2(n_\omega+n_{2\omega})}\right)}$$

$$= \frac{4\pi^2L^2}{\lambda^2}\left(\frac{d_s}{d_{Qtz}}\right)^2\frac{t_\omega^4 T_{2\omega}}{(2n_\omega\cos\theta'_{PM})^2}\times \left[\frac{(1+n_{Qtz}^{\omega})^3(1+n_{Qtz}^{2\omega})^3(n_{Qtz}^{\omega}-n_{Qtz}^{2\omega})^2(n_{Qtz}^{\omega}+n_{Qtz}^{2\omega})}{n_{Qtz}^{2\omega}}\right] \quad \text{(A8)}$$

Acknowledgment. S.L. thanks EPSRC for a studentship.

References and Notes

(1) Twieg, R.; Azema, A.; Jain, K.; Cheng, Y. *Chem. Phys. Lett.* **1982**, *92*, 208.

(2) Bailey, R. T.; Cruickshank, F. R.; Guthrie, S. M. G.; McArdle, B. J.; Morrison, H.; Pugh, D.; Shepherd, E. A.; Sherwood, J. N.; Yoon, C. S.; Kashyap, R.; Nayar, B. K.; White, K. I. *Opt. Commun*. **1988**, *65*, 229.

(3) Kondo, T.; Morita, R.; Ogasawara, N.; Umegaki, S.; Ito, R. *Jpn. J. Appl. Phys.* **1989**, *28*, 1622.

(4) Tweig, R. J.; Dirk, C. W.; Report RJ 5237154077; IBM: , 1986.

(5) Bailey, R. T.; Cruickshank, F. R.; Kerkoc, P.; Pugh, D.; Sherwood, J. N. *Appl. Opt.* **1995**, *34*, 1239.

(6) Lochran, S.; Bailey, R. T.; Cruickshank, F. R.; Pugh, D.; Sherwood, J. N.; Simpson, G. S.; Wallis, J. D.; Langley, P. J. *J. Phys. Chem. A* **1998**, *102*, 8520.

(7) Bailey, R. T.; Blaney, S.; Cruickshank, F. R.; Guthrie, S. M. G.; Pugh, D.; Sherwood, J. N. *Appl. Phys. B* **1988**, *47*, 83.

(8) Kurtz, S. K.; Perry, T. T. *J. Appl. Phys.* **1968**, *39*, 3798.

(9) Bergman, J. G.; Crane, G. R.; Levine, B. F.; Bethea, C. G. *Appl. Phys. Lett.* **1972**, *20*, 21.

(10) Tsunekawa, T.; Gotoh, T.; Iwamoto, M. *Chem. Phys. Lett.* **1990**, *166*, 353.

(11) Jerphagnon, J.; Kurtz, S. K. *J. Appl. Phys.* **1970**, *41*, 1667.

(12) Zyss, J.; Chemla, D. S.; Nicoud, J. F. *J. Chem. Phys.* **1981**, *74*, 4800.

(13) Jerphagnon, J.; Kurtz, S. K. *Phys. Rev. B:* **1970**, *1*, 1739.

(14) (a) Oudar, J. L.; Chemla, D. S. *J. Chem. Phys.* **1977**, *66*, 2664. (b) Tomaru, S.; Matsumoto, S.; Kurihara, T.; Suzuki, H.; Ooba, N.; Kaino, T. *Appl. Phys. Lett.* **1991**, *58*, 2583.

(15) Hagimoto, K.; Mito, A. *Appl. Opt.* **1995**, *34*, 8276.

(16) Roberts, D. A. *IEEE J. Quantum Electron*. **1992**, *28*, 2057.

(17) Zyss, J.; Oudar, J. L. *Phys. Rev. A: At., Mol., Opt., Phys.* **1982**, *26*, 2028.

(18) Pugh, D.; Morley J. O. In *Nonlinear Optical Properties of Organic Molecules and Crystals*; Chemla, D. S., Zyss, J., Eds.; Academic Press: 1987; Vol 1, p 193.

(19) Kondo, T.; Akase, F.; Kumagai, M.; Ito, R. *Opt. Rev.* **1995**, *2*, 128.

(20) Nayar, B. K.; Kashyap, R.; White, K. I.; Bailey, R. T.; Cruickshank, F. R.; Guthrie, S. M. G.; McArdle, B. J.; Morrison, H.; Pugh, D.; Shepherd, E. E. A.; Sherwood, J. N.; Yoon, C. S. *S.P.I.E. Proc.* **1988**, *971*, 76.